J Appl Physiol 104: 218–223, 2008.
First published November 15, 2007; doi:10.1152/japplphysiol.00301.2007.

Left ventricular dysfunction and associated cellular injury in rats exposed to chronic intermittent hypoxia

Ling Chen,[1] Jin Zhang,[2] Tracey X. Gan,[3] Ye Chen-Izu,[4] Jeffrey D. Hasday,[1] Morris Karmazyn,[3] C. William Balke,[4,5] and Steven M. Scharf[1]

[1]*Division of Pulmonary and Critical Care Medicine and* [2]*Department of Physiology, University of Maryland, Baltimore, Maryland;* [3]*Department of Physiology and Pharmacology, University of Western Ontario, London, Ontario, Canada; and Departments of* [4]*Internal Medicine and* [5]*Physiology, University of Kentucky College of Medicine, Lexington, Kentucky*

Submitted 16 March 2007; accepted in final form 5 November 2007

Chen L, Zhang J, Gan TX, Chen-Izu Y, Hasday JD, Karmazyn M, Balke CW, Scharf SM. Left ventricular dysfunction and associated cellular injury in rats exposed to chronic intermittent hypoxia. *J Appl Physiol* 104: 218–223, 2008. First published November 15, 2007; doi:10.1152/japplphysiol.00301.2007.—Obstructive sleep apnea (OSA) increases cardiovascular morbidity and mortality. We have reported that chronic intermittent hypoxia (CIH), a direct consequence during OSA, leads to left ventricular (LV) remodeling and dysfunction in rats. The present study is to determine LV myocardial cellular injury that is possibly associated with LV global dysfunction. Fifty-six rats were exposed either to CIH (nadir O_2 4–5%) or sham (handled normoxic controls, HC), 8 h/day for 6 wk. At the end of the exposure, we studied LV global function by cardiac catheterization, and LV myocardial cellular injury by in vitro analyses. Compared with HC, CIH animals demonstrated elevations in mean arterial pressure and LV end-diastolic pressure, but reductions in cardiac output (CIH 141.3 ± 33.1 vs. HC 184.4 ± 21.2 $ml \cdot min^{-1} \cdot kg^{-1}$, $P < 0.01$), maximal rate of LV pressure rise in systole ($+dP/dt$), and maximal rate of LV pressure fall in diastole ($-dP/dt$). CIH led to significant cell injury in the left myocardium, including elevated LV myocyte size, measured by cell surface area (CIH 3,564 ± 354 vs. HC 2,628 ± 242 μm^2, $P < 0.05$) and cell length (CIH 148 ± 23 vs. HC 115 ± 16 μm, $P < 0.05$), elevated terminal deoxynucleotidyl transferase-mediated dUTP nick end labeling (TUNEL)-stained positive cell number (CIH 98 ± 45 vs. HC 15 ± 13, $P < 0.01$), elevated caspase-3 activity (906 ± 249 vs. 2,275 ± 1,169 $pmol \cdot min^{-1} \cdot mg^{-1}$, $P < 0.05$), and elevated expression of several remodeling gene markers, including c-fos, atrial natriuretic peptide, β-myosin heavy chain, and myosin light chain-2. However, there was no difference between groups in sarcomere contractility of isolated LV myocytes, or in LV collagen deposition on trichrome-stained slices. In conclusion, CIH-mediated LV global dysfunction is associated with myocyte hypertrophy and apoptosis at the cellular level.

obstructive sleep apnea; cardiac hypertrophy; apoptosis

OBSTRUCTIVE SLEEP APNEA (OSA) is a common and serious disease. It affects 4–6% of men and 2–4% of women (38), with higher prevalence in elderly and overweight individuals, and increases morbidity and mortality attributable to hypertension, coronary artery disease, congestive heart failure with myocardial hypertrophy and remodeling, and stroke (29, 30). OSA demonstrates repetitive upper airway occlusion during sleep, which directly causes chronic intermittent hypoxia (CIH), exaggerated swing of intrathoracic pressure, and arousal (33). In rodents, CIH induces several cardiovascular features seen in patients with OSA, including hypertension, sympathetic activation, ventricular hypertrophy (1–3, 5, 8–13, 16, 17, 23, 26, 27, 35), and left ventricular (LV) global dysfunction (5). These animal studies suggest an important role of CIH in cardiovascular pathogenesis during the development of OSA.

The current concept of ventricular remodeling in heart disease includes classically defined ventricular enlargement, and additional pathological events at the cellular and molecular levels (15, 25). Indeed, several cellular and molecular changes have been suggested to be involved in the development of the ventricular remodeling and dysfunction, including cardiomyocyte hypertrophy and apoptosis (7, 22), myocardial inflammation and fibrosis (7, 21, 28), "isoform switching" of contractile proteins (19), and changes in the profile of myocardial gene expression (18). However, to the best of our knowledge, there are few studies investigating cellular and molecular changes in CIH-exposed hearts. Such studies would provide additional information on the pathogenesis of the cardiovascular dysfunction in OSA.

Our previous study in CIH (5) demonstrated increased LV weight and LV dysfunction at the whole organ level. Factors accounting for these findings could include hypertrophy and/or poor contractility of individual myocytes, loss of myocytes due to apoptosis and/or necrosis, infiltration of inflammatory cells, and changes in extracellular matrix such as collagen deposition. There are few data available on cellular and molecular concomitants of cardiac injury in the CIH model. In the present study we specifically examined cellular markers of LV injury, including cardiomyocyte hypertrophy and contractile function, apoptosis, collagen deposition, and changes in expression of several remodeling gene markers that accompany changes in LV global function. We hypothesized that CIH-induced LV global dysfunction is associated with LV cellular injury, manifesting as cellular hypertrophy, apoptosis, poor contractility, collagen deposition, and elevated mRNA expression of selected remodeling genes.

METHODS

In accordance with approval from the Institutional Animal Care and Use Committee of University of Maryland, 56 male Sprague-Dawley rats (175–200 g) with constant food and water access were randomized on a 1:1 basis into experimental (CIH) and similarly handled normoxic control (HC) groups.

Address for reprint requests and other correspondence: L. Chen, Div. of Pulmonary and Critical Care Medicine, Dept. of Medicine, Univ. of Maryland, Baltimore, 685 West Baltimore St., MSTF 816, Baltimore, MD 21201 (e-mail: Lchen@medicine.umaryland.edu).

The costs of publication of this article were defrayed in part by the payment of page charges. The article must therefore be hereby marked "*advertisement*" in accordance with 18 U.S.C. Section 1734 solely to indicate this fact.

CIH and sham exposure. As previously described (5), during the exposure periods animals were housed in 2.5-liter Plexiglas chambers of an environment system (HypOxyc system, Kent Scientific, Torrington, CT). Animals in the chambers were allowed free mobility, and water and food were provided ad libitum. The O_2 concentration in each chamber was continuously monitored, and the degree and timing of hypoxia were manipulated by computer-driven servo-controlled solenoids that regulate the timing and flow rate of N_2 and room air through the chambers. Each cycle of intermittent hypoxia lasted for ~2 min, with the first minute being the hypoxia exposure phase, and the following minute being the reoxygenation phase. During the hypoxia phase, ambient O_2 concentration in the chambers was rapidly decreased to 4–5% at nadir by varying the N_2 flush times and flow rate. The nadir O_2 lasted for 15–20 s per the cycle. During the reoxygenation phase, O_2 concentration was turned up to 21% at maximum by rapid flushing with room air.

To characterize blood gas tensions over the course of these experiments, three additional animals were anesthetized with 1.5% isoflurane, the right femoral artery was cannulated, and arterial blood samples were collected at the following timing points: baseline (before intermittent hypoxia), during the nadir O_2 in the 3rd, 5th, and 6th hypoxia phase, and during the 3rd, 4th, and 6th reoxygenation phase. Results of blood gases were *1*) at baseline: pH 7.41 ± 0.02, P_{O_2} 98 ± 4 mmHg, and P_{CO_2} 43 ± 2 mmHg; *2*) during the hypoxia phase: pH 7.48 ± 0.02, P_{O_2} 44 ± 8 mmHg, P_{CO_2} 32 ± 2 mmHg; and *3*) during the reoxygenation phase: pH 7.41 ± 0.01, P_{O_2} 75 ± 13 mmHg, and P_{CO_2} 39 ± 2 mmHg. The results indicate that our protocol led to moderate to severe hypoxia, in the range seen in patients with moderate to severe OSA (30).

The intermittent hypoxia was performed daily for 8 daylight hours (1000–1800) for 6 wk. Following the exposure, animals were returned to their usual cages in the animal housing facility. HC animals were handled similarly as the CIH animals, except exposed to a continuous flow of room air. Data, as described below, were collected at the end of the 6 wk, in the next morning after the last exposure, to minimize acute effects of intermittent hypoxia.

Hemodynamics and LV function. Cardiac catheterization was performed under anesthesia with 2.5% isoflurane (5). Two micromanometer-tipped catheters (2.5-Fr, Millar Instruments, Houston, TX) were inserted into the left ventricle and the superior vena cava, respectively, via cutdowns of the right carotid artery and the right jugular vein, respectively. LV pressure and central venous pressure were measured following a 20-min stabilization period under 1.5% isoflurane. The LV catheter was then pulled back to the ascending aorta for measurement of arterial pressure. The two catheters were then replaced, respectively, with a 2.5-Fr thermistor (Edward Lifesciences, Irvine, CA) into the ascending aorta and a PE-20 tubing onto the right atrium. Cardiac output was measured with thermodilution (Vigilance, Edward Lifesciences) by 0.2 ml of cold saline injection into the right atrium and blood temperature sampling from the aorta. Three reproducible measurements, which were defined as being within 15% of each other, were averaged. The reading was further calibrated by multiplying by a factor that was established in preliminary studies, in which cardiac output was measured simultaneously by the thermodilution method and a method using chronically implanted flow probe (Transonics System, Ithaca, NY) in the ascending aorta. Data obtained by catheterization include arterial blood pressure, cardiac output, LV end-diastolic pressure, and maximal rate of LV pressure rise in systole ($+dP/dt$) and maximum rate of LV pressure fall in diastole ($-dP/dt$).

Collection of heart specimens. Following cardiac catheterization, animals were deeply anesthetized by 5% isoflurane, and the hearts were rapidly excised. The aorta was cannulated retrogradely and immediately perfused with cold saline. The hearts were used for the following analyses: *1*) isolated myocyte studies (5 animals for HC and 6 for CIH); *2*) histological study (6 animals each group); *3*) caspase-3 activity (6 animals each group); and *4*) gene expression (6 animals each group).

Cardiomyocyte isolation and measurements. Myocytes were isolated using a previously described method (4) with modification. The hearts were perfused for 20–30 min with physiological salt-containing solution [PSS; in mM: 135 NaCl, 4 KCl, 0.33 $NaHPO_4$, 1 $MgSO_4$, 10 HEPES, 10 glucose, and 1.8 $CaCl_2$; containing 0.9 mg/ml of type II collagenase (Sigma-Aldrich, St. Louis, MO)]. LV free wall tissue was then minced, and myocytes were dissociated by gently shaking at 30°C. The cells were sequentially washed and resuspended in PSS with gradually increased Ca^{2+} concentrations (0.4, 0.6, 0.8, until 1.0 mM).

For cell size measurement, cells were bathed in PSS and allowed to settle onto a laminin-coated glass coverslip heated to 37°C. The coverslip was placed on the bottom of perfusion bath and mounted on an inverted microscope (Digi2, LaboAmerica, Fremont, CA). Cell length, width, and cross surface area were measured from digital images with SigmaScan Pro (SysStat Software, Point Richmond, CA). For each heart, we measured 100 quiescent myocytes that were rod shape with clear Z-lines.

Contractility of isolated myocytes was studied in vitro under unloaded conditions (6). The cells were bathed on a coverslip in PSS at 37°C. Cells were oriented with their longitudinal axis parallel to the long axis of the microscope focal plane. Cell contraction was induced by field stimulation (4 ms, 5–15 V, and 1 Hz). Transmitted light images of the cell were digitalized and recorded via an IonOptix system (IonOptix, Milton, MA). A Fast Fourier transform algorithm was used for measurement of sarcomere spacing from the optical density across the sarcomeres. Figure 1 shows an example of the tracings. For purpose of quality control, cells with resting sarcomere length no less than 1.75 mm were chosen.

LV histology. Hearts were fixed in 10% formalin saline (pH 7.4) overnight, embedded in paraffin, and serially sectioned into 5-μm slices perpendicular to its long axis. Standard hematoxylin and eosin (HE) staining was performed for routine histology, and Gomori's trichrome staining was performed for deposition of collagen that was stained as blue.

Apoptosis assays. We examined whether CIH leads to increased apoptosis in LV myocardium, using terminal deoxynucleotidyl transferase-mediated dUTP nick end labeling (TUNEL) staining of heart slice and spectrophotometric measurement of caspase-3 activity of LV cell extracts. TUNEL staining was performed on the heart slices using

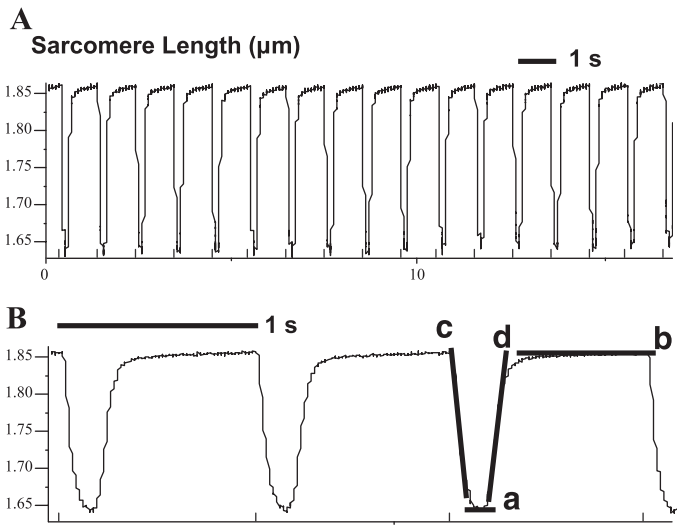

Fig. 1. Representative recording (*A*) and data analysis diagram (*B*) of sarcomere length during stimulated contraction. The load-free left ventricular (LV) cardiomyocyte was isolated from a handled normoxic control (HC) animal. *a* = systolic sarcomere length; *b* = diastolic (resting) sarcomere length; Slope of *line c* = sarcomere contraction velocity; slope of *line d* = sarcomere relaxation velocity. Fractional shortening (%) = $[(b - a)/b] \times 100$.

TdT-FragEL apoptosis detection kits (Calbiochem, San Diego, CA) according to the manufacturer's instructions. Counterstaining with methyl green aided in the morphological evaluation of normal and apoptotic nuclei, in which normal nuclei were stained as blue and apoptotic nuclei as brown. The number of TUNEL-positive cells within a 2.5-mm^2 field in LV free wall was counted, and eight randomly selected fields per slide and five sections per hearts were averaged for statistical analysis. The observer was blinded to the treatment group.

For measurement of caspase-3 activity in cell homogenates, freshly collected LV free wall tissues were minced, homogenized at 4°C with 1 ml of PBS, and centrifuged with 10,000 *g* at 4°C for 20 min. The supernatants (e.g., cellular extracts) were collected for caspase-3 activity with caspase-3 cellular activity assay kit (cat. no. 235,419, Calbiochem) under the manufacture's instruction. In brief, 10 μl of LV extract was mixed with 40 μl assay buffer consisting of 100 mM NaCl, 50 mM HEPES, 10 mM DTT, 1 mM EDTA, 10% glycerol, 0.1% CHAPS, pH 7.4. The mixture was reacted with 50 μl caspase-3 substrate I containing 200 μM of Ac-DEVD-pNA, and the absorbance was measured at 405 nM at 5-min intervals for 120 min. The triplicate results from the same LV sample were averaged and normalized to the protein content.

mRNA expression of hypertrophy-associated biomarkers. As described previously (37), LV free wall was dissected and homogenized in Trizol reagent (Invitrogen, Burlington, ON, Canada). RNA was recovered from the aqueous phase following centrifugation. First-strand cDNA was synthesized using the Superscript-II system (Invitrogen). Real-time PCR was performed in 20-μl reaction volumes using SYBR green JumpStart *Taq* ReadyMix DNA polymerase (Sigma-Aldrich). Fluorescence was measured with a DNA Engine Opticon 2 system (MJ Research, Waltham, MA). PCR conditions and cycle number were optimized for each set of primers that represented atrial natriuretic peptide (ANP), β-myosin heavy chain (β-MHC), myosin light chain-2 (MLC2), and 18S RNA. Results were presented as the ratio of the interested gene to 18S RNA, a housekeeping gene. The upregulation of these genes has been well documented in other LV hypertrophy models (18).

Statistics. All the data showed a normal distribution as determined by Kolmogorov-Smirnov test. Data were compiled and presented as means ± SD. Unpaired *t*-test was used to test for significance. The null hypothesis was rejected at the 5% level.

RESULTS

Body weight, hemodynamics, and LV global function. Table 1 summarizes body weight and catheterization data measured at the end of the 6-wk exposure. There were no differences between the groups in baseline body weight (HC 195 ± 23 g vs. CIH 193 ± 28 g; $P > 0.05$), or in weight gain over the 6-wk experimental period (HC 148 ± 17 g vs. CIH 156 ± 22 g; $P > 0.05$). Mean arterial pressure, LV end-diastolic pressure, and systemic vascular resistance were significantly greater in CIH compared with the HC group. Cardiac output and stroke volume (both were expressed per kg body weight), and LV +dP/d*t* and −dP/d*t* were significantly lower in CIH than in the HC group. There were no significant differences in heart rate between the groups.

Table 1. *Body weight, hemodynamics, and LV function*

Variables	HC	CIH
BW gain, g	156±22	148±17
MAP, mmHg	98.2±8.6	115.1±10.3*
HR, beats/min	321±28	333±37
LVEDP, mmHg	7.4±3.8	12.7±6.1*
CO/BW, ml·min^{-1}·kg^{-1}	184.4±21.2	141.3±33.1†
SV/BW, ml/kg	0.54±0.08	0.39±0.11†
SVR, mmHg·ml^{-1}·min	1.55±0.32	2.41±0.78†
+dP/d*t*, mmHg/s	6,983±1,119	5,238±1,974*
−dP/d*t*, mmHg/s	−8,665±1,238	−5,142±2,322†

Data are means ± SD from 44 animals (22 animals each group). CIH, chronic intermittent hypoxia; HC, handled normoxic controls; BW gain, body weight gain at the end of 6-wk experiment from baseline; MAP, mean arterial pressure; HR, heart rate; LVEDP, LV end-diastolic pressure; CO, cardiac output; SV, stroke volume; SVR, systemic vascular resistance = (MAP/CO); +dP/d*t*, maximal rate of LV pressure rise in systole; −dP/d*t*, maximal rate of LV pressure fall in diastole. *$P < 0.05$, †$P < 0.01$ compared with HC via unpaired *t*-test.

Size and contractile function of isolated LV cardiomyocytes. As shown in Fig. 2, *A* and *B*, respectively, the surface area and length of unloaded and resting myocytes were significantly greater in CIH than in HC animals, which was consistent with the presence of cardiac hypertrophy in the former as observed previously at the whole-heart level (5). However, cell width was not significantly different between the groups (HC 23.2 ± 3.4 μm vs. CIH 24.6 ± 5.3 μm; $P > 0.05$). Representative images of isolated myocytes are shown in Fig. 2*C*.

Figure 1*A* shows representative recordings of sarcomere contraction induced by electrical field stimulation in a HC myocytes. Figure 1*B* demonstrates the methods for the calculation of sarcomere parameters. As shown in Table 2, there were no significant differences between CIH and HC in any sarcomere parameters, including systolic and diastolic length, fractional shortening, and contraction and relaxation velocity.

LV routine histology. No differences were observed between the CIH and HC groups in histological examination of the HE- or trichrome-stained heart slices. Specifically, there was no evidence in either group for myocyte necrosis or leukocyte infiltration in HE-stained slices, and no differences in the pattern of collagen deposition were observed in trichrome-stained slices.

Apoptosis assays. As shown in Fig. 3*A*, the number of TUNEL-positive cells from the CIH group was approximately fivefold greater compared with the HC group ($P < 0.05$). The elevated LV apoptosis is further supported by twofold increases in caspase-3 activity in LV cell extracts from CIH group compared with that from HC group ($P < 0.02$), as shown as Fig. 3*B*.

LV expression of remodeling marker genes. LV myocardial expression of four genes was measured by real-time PCR, including c-fos, an early response gene, and three fetal genes, e.g., ANP, β-MHC, and MLC2. As shown in Fig. 4, all four genes were significantly upregulated in CIH animals, including a 1.5-fold increases in ANP, and ~10-fold increases in the three other genes.

DISCUSSION

As in our previous study (5), the present results showed elevated blood pressure and LV dysfunction in rats exposed to CIH compared with controls. Most important, animals exposed to CIH demonstrated a number of cellular and molecular changes known to be associated with global myocardial injury, including hypertrophy, apoptosis, and elevated mRNA expression of remodeling gene markers. To the best of our knowledge, there are few previous reports of these findings in the literature.

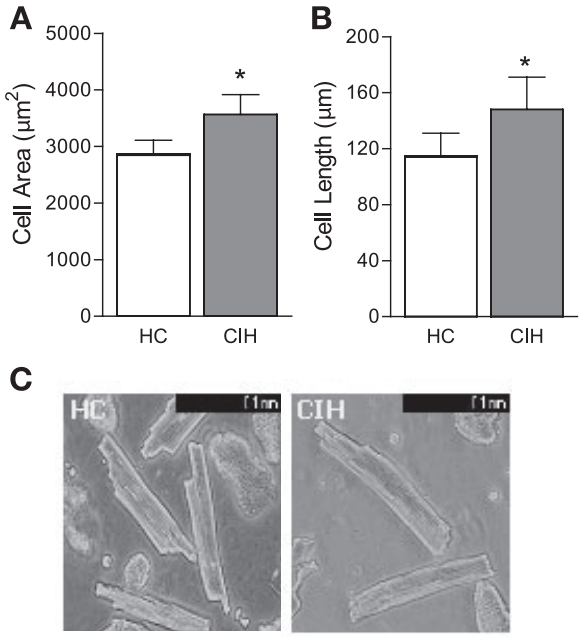

Fig. 2. Cell size of isolated LV cardiomyocytes. Compared with HC, chronic intermittent hypoxia (CIH) group shows significant increases in both cross surface area (*A*) and cell length (*B*) $*P < 0.05$, 6 animals per group, data from the same heart were averaged before significance test with unpaired *t*-test. *C*: representative images of isolated LV cardiomyocytes from a HC (*left*) and a CIH (*right*) heart.

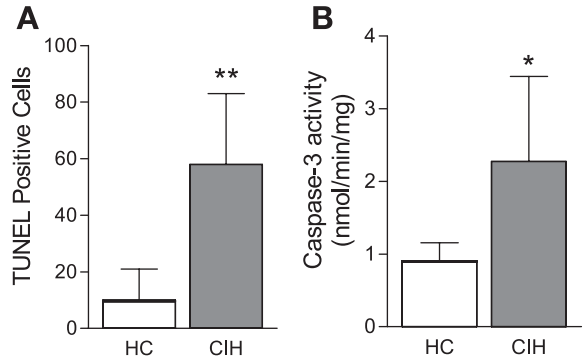

Fig. 3. Apoptosis assays. *A*: terminal deoxynucleotidyl transferase-mediated dUTP nick end labeling (TUNEL) assay of formalin-fixed and paraffin-embedded heart slices. Compared with HC, CIH group shows significant increases in TUNEL-positive cells in the myocardium of LV free wall ($**P < 0.01$, $n = 6$ hearts each group). The TUNEL-positive cells within a 2.5-mm² field in LV free wall were counted and averaged from 8 randomly selected fields per slide and 5 sections per heart. *B*: caspase-3 activity measured in cell extracts of freshly collected LV free wall tissues. CIH group shows significant increases in caspase-3 activity compared with HC group ($*P < 0.05$, $n = 6$ hearts each group).

Global LV dysfunction. Rodent models of CIH mimic several cardiovascular features seen in OSA patients, including blood pressure elevation (1–3, 5, 9–13), and LV hypertrophy indicated by changes in heart wet weight (3, 5, 9–12, 23) and LV posterior wall thickness (5). Increased right ventricular weight has also been observed in some (8, 26, 27) but not in all reports (1, 2, 5, 9–12). Consistent with our previous report (5), the present study demonstrated signs of global LV dysfunction in CIH animals, including increased LV end-diastolic pressure, decreased cardiac output/body weight, and decreased LV $+dP/dt$ and $-dP/dt$ (Table 1). Blood pressure elevation in CIH is likely caused by sympathetic hyperactivation contributable to increased chemoreceptor stimulation from hypoxia (5, 9, 11, 17, 33). The mechanisms for LV injury are not well understood; however, changes in blood pressure and sympathetic tone are unlikely to be responsible. Blood pressure elevation in CIH was small (only 17%, relative to HC), whereas LV dysfunction was rather large, as suggested by a 35% decreases in stroke volume/body weight. Furthermore, chronic sympathetic denervation eliminated CIH-induced blood pressure changes but not the occurrence of LV hypertrophy (11). Therefore myocardial injury in CIH likely results from the direct effects of repetitive hypoxia and reoxygenation. Indeed, myocardial oxidative stress occurred in CIH (5, 29), and caused myocyte hypertrophy and apoptosis in cultured cardiomyocytes (32). We speculate that oxidant stress may trigger LV

Table 2. *Pooled data of sarcomere length variables from the isolated and unloaded LV cardiomyocytes under field electrical stimulation*

	HC	CIH
Sample size	42 cells from 5 rats	47 cells from 6 rats
Diastolic length, μm	1.86±0.03	1.86±0.03
Systolic length, μm	1.63±0.06	1.65±0.03
Fractional shortening, %	11.4±2.0	11.3±1.25
Maximal contraction velocity, μm/μs	−3.44±0.81	−3.18±0.47
Maximal relaxation velocity, μm/μs	2.85±0.93	2.51±0.47

Data are means ± SD. Data from same hearts were averaged before significance test with unpaired *t*-test. Fractional shortening (%) = [(diastolic length − systolic length)/diastolic length] × 100. There were no significant differences ($P > 0.05$) between groups in any variables.

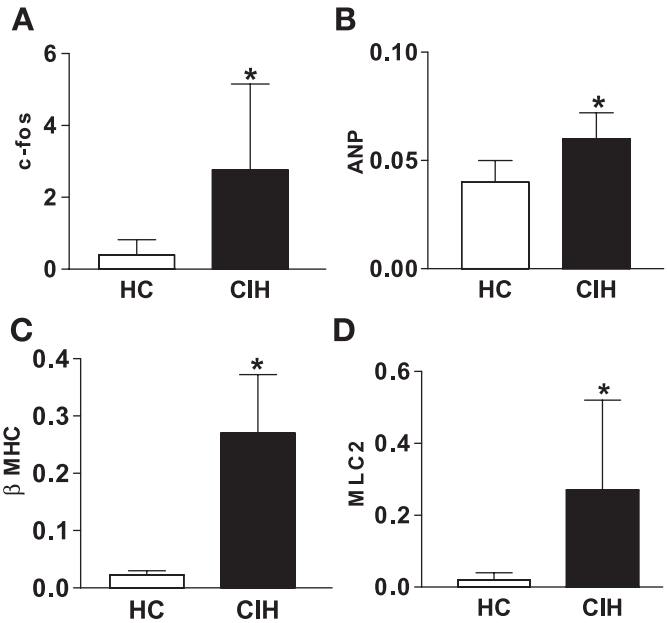

Fig. 4. mRNA expression of selected genes in LV free wall tissue, measured by real-time PCR. Compared with HC, CIH group demonstrates significantly upregulated expressions of c-fos (*A*), atrial natriuretic peptide (ANP, *B*), β-myosin heavy chain (β-MHC, *C*), and myosin light chain-2 (MLC2, *D*). All the data are expressed as the ratio to 18S rRNA; $*P < 0.05$ between HC and CIH; $n = 6$ each group.

hypertrophy observed globally and on the cellular level in this study.

Myocyte hypertrophy and contraction. Myocardial hypertrophy predicts an adverse outcome in patients with heart diseases, such as increased cardiac mortality (24). Antihypertrophic therapy improves cardiac dysfunction and outcome in patients and animal models (14). Since both LV hypertrophy and dysfunction are evident in CIH rats, as demonstrated in the present and previous paper (5), hypertrophy likely contributes to the development of LV dysfunction. In the present study, we observed an increase of ~21% in LV myocyte area in CIH compared with HC (Fig. 2). This suggests myocyte hypertrophy likely among the cellular bases for the increased LV weight observed in previous studies (3, 5, 9–12, 24). Moreover, the CIH-induced elevation in LV myocyte area is relatively greater than that in LV weight (11% compared with HC) that we reported previously using the same protocol (5), suggesting that other cellular changes, such as loss of myocytes, have offset the effect of myocyte hypertrophy with regard to the changes in LV weight. Indeed, as discussed below, we observed an increased apoptosis, but no signs of inflammatory infiltration and collagen deposition in LV myocardium.

CIH caused no significant changes in diastolic and systolic sarcomere length of LV cardiomyocytes (Table 2), suggesting cardiomyocyte elongation in this model was primarily due to an increased number of sarcomeres, rather than lengthening of existing sarcomeres. Indeed, sarcomere length (either systolic or diastolic) at the cellular level is primarily determined by calcium homeostasis, myofilament sensitivity to calcium, and the number of cross bridges that are formed (20).

CIH group shows no significant change in the fractional shortening of sarcomeres (Table 2) that measures myocyte contractile function. However, a previous study in spontaneously hypertensive rats (SHR) (34) showed that myocyte hypertrophy was associated with an enhanced contractility at both whole organ and cellular levels. The observed differences in myocyte contractility between models of CIH and SHR may represent differences in the underlying mechanisms initiating hypertrophy and/or the progression stages of the myocyte hypertrophy. Indeed, LV injury in SHR results from increases in LV afterload, whereas, as noted above, we do not believe that this was the case with the CIH model. It is unclear why CIH animals, compared with HC, had global LV pump dysfunction but preserved sarcomere contractility. While technical limitations confounding isolated myocyte study (see below) cannot be excluded completely, it is more likely that LV global dysfunction is caused by cellular mechanisms other than sarcomere contractile dysfunction of the surviving myocytes. Possibilities including cardiomyocyte apoptosis, and myocardial fibrosis and inflammation are discussed below.

Myocardial apoptosis and histology. CIH group demonstrated significant apoptosis in LV myocardium (Fig. 3), as indicated by increased TUNEL-positive myocytes and caspase-3 activity. Consistently, it has been shown that upregulated proapoptotic proteins and downregulated antiapoptotic proteins in chronic sustained hypoxia (8 h/day for 4–8 wk) (23). Myocardial apoptosis contributes to myocardial damage in cultured myocytes exposed to hypoxia (36), postinfarct remodeling in rodents (22), and patients with heart failure (7). While apoptosis may also play an important role in LV dysfunction in CIH, however, its exact contribution as well as the initial mechanisms is still to be determined. In CIH mice, oxidative stress caused neuronal apoptosis (38). Consistently, we observed in CIH rats a correlation between the degree of myocardial oxidative stress and LV dysfunction (5). It is therefore possible that oxidative stress may be an initiator of apoptosis in this model.

Myocardial inflammation and fibrosis have been observed in animal models and patients with heart disease (7, 21, 28). In the present study, however, we did not observe any histological evidence of myocardial inflammation or fibrosis on either HE- or trichrome-stained heart slices from CIH animals, suggesting that their role in this model is likely small.

Gene expression. Myocardial remodeling is associated with upregulation in myocardial expression of embryonic gene isoforms (18, 19). For example, c-fos expression elevated in the myocardium during the early phase of LV overload (18), and also in the brain stem in CIH-exposed rodents (16, 38). The other fetal gene upregulation was usually observed at the hypertrophic-failing phase (18). As Fig. 4 shows, CIH animals demonstrated a coexistence of early (e.g., c-fos) and late (e.g., ANP, β-MHC, and MLC2) gene markers of cardiac remodeling. This molecular characteristic may suggest a sustained LV injury over CIH exposure and thus underlie an accelerated deterioration of LV function in this model. Indeed, except as molecular markers of cardiac remodeling, chronically activated fetal gene profiles may actually trigger pathological changes leading to myocardial dysfunction (18).

Limitations. This study needs to be interpreted within the context of several potential limitations. First, cardiomyocytes underwent a short period of ischemia and reperfusion during cell isolation, which might have selected out those myocytes with good sarcomere contractile function. Second, cardiomyocyte contraction was studied under unloaded conditions, which might be different from that under loaded conditions in vivo (31). Last, patients with OSA are exposed to CIH with hypercapnia for years, rather than CIH with hypocapnia for weeks in this study. It is possible that longer exposures might have strengthened or lessened the degree of the myocardial injury observed in this study.

Conclusions. CIH-induced global LV dysfunction was accompanied by cellular and molecular changes, including cardiomyocyte hypertrophy, apoptosis, and changed profile of gene expression, although there was no significant change in sarcomere contractile function. We speculate that the global dysfunction can be explained, in part, by hypertrophy and apoptosis at the cardiomyocyte level.

GRANTS

This study was supported by an intramural grant from the University of Maryland School of Medicine (L. Chen), American Heart Association Grants 0765262U and 0655487U (L. Chen and S. M. Scharf), a grant from the Maryland Thoracic Society (S. M. Scharf), and National Heart, Lung, and Blood Institute RO1 Grants HL-071865 and HL-68733 (C. W. Balke).

REFERENCES

1. **Bao G, Randhawa PM, Fletcher EC.** Acute blood pressure elevation during repetitive hypocapnic and eucapnic hypoxia in rats. *J Appl Physiol* 82: 1071–1078, 1997.
2. **Bao G, Metreveli N, Li R, Taylor A, Fletcher EC.** Blood pressure response to chronic episodic hypoxia: role of the sympathetic nervous system. *J Appl Physiol* 83: 95–101, 1997.

3. **Campen MJ, Shimoda LA, O'Donnell CP.** Acute and chronic cardiovascular effects of intermittent hypoxia in C57BL/6J mice. *J Appl Physiol* 99: 2028–2035, 2005.
4. **Chen L, Chen CX, Gan XT, Beier N, Scholz W, Karmazyn M.** Inhibition and reversal of myocardial infarction-induced hypertrophy and heart failure by NHE-1 inhibition. *Am J Physiol Heart Circ Physiol* 286: H381–H387, 2004.
5. **Chen L, Einbinder E, Zhang Q, Hasday J, Balke CW, Scharf SM.** Oxidative stress and left ventricular function with chronic intermittent hypoxia in rats. *Am J Respir Crit Care Med* 172: 915–920, 2005.
6. **Chen-Izu Y, McCulle SL, Ward CW, Soeller C, Allen BM, Rabang C, Cannell MB, Balke CW, Izu LT.** Three-dimensional distribution of ryanodine receptor clusters in cardiac myocytes. *Biophys J* 91: 1–13, 2006.
7. **Diez J, Gonzalez A, Lopez B, Querejeta R.** Mechanisms of disease: pathologic structural remodeling is more than adaptive hypertrophy in hypertensive heart disease. *Nat Clin Pract Cardiovasc Med* 2: 209–216, 2005.
8. **Fagan KA.** Pulmonary hypertension in mice following intermittent hypoxia. *J Appl Physiol* 90: 2502–2507, 2001.
9. **Fletcher EC, Lesske J, Behm R, Miller CC 3rd, Stauss H, Unger T.** Carotid chemoreceptors, systemic blood pressure, and chronic episodic hypoxia mimicking sleep apnea. *J Appl Physiol* 72: 1978–1984, 1992.
10. **Fletcher EC, Lesske J, Qian W, Miller CC 3rd, Unger T.** Repetitive, episodic hypoxia causes diurnal elevation of blood pressure in rats. *Hypertension* 19: 555–561, 1992.
11. **Fletcher EC, Lesske J, Culman J, Miller CC, Unger T.** Sympathetic denervation blocks blood pressure elevation in episodic hypoxia. *Hypertension* 20: 612–619, 1992.
12. **Fletcher EC, Bao G, Miller CC 3rd.** Effect of recurrent episodic hypocapnic, eucapnic, and hypercapnic hypoxia on systemic blood pressure. *J Appl Physiol* 78: 1516–1521, 1995.
13. **Fletcher EC, Orolinova N, Bader M.** Blood pressure response to chronic episodic hypoxia: the renin-angiotensin system. *J Appl Physiol* 92: 627–633, 2002.
14. **Frey N, Katus HA, Olson EN, Hill JA.** Hypertrophy of the heart: a new therapeutic target? *Circulation* 109: 1580–1589, 2004.
15. **Gerdes AM, Kellerman SE, Moore JA, Muffly KE, Clark LC, Reaves PY, Malec KB, McKeown PP, Schocken DD.** Structural remodeling of cardiac myocytes in patients with ischemic cardiomyopathy. *Circulation* 86; 426–430, 1992.
16. **Greenberg HE, Sica A, Batson D, Scharf SM.** Chronic intermittent hypoxia increases sympathetic responsiveness to hypoxia and hypercapnia. *J Appl Physiol* 86: 298–305, 1999.
17. **Greenberg HE, Sica AL, Scharf SM, Ruggiero DA.** Expression of c-fos in the rat brainstem after chronic intermittent hypoxia. *Brain Res* 816: 638–645, 1999.
18. **Hoshijima M, Chien KR.** Mixed signals in heart failure: cancer rules. *J Clin Invest* 109: 849–855, 2002.
19. **Katz AM.** Heart failure. In: *Physiology of the Heart* (3rd ed.), edited by Katz AM. Philadelphia, PA: Lippincott Williams and Wilkins, 2001, p. 658–94.
20. **Kobayashi T, Solaro RJ.** Calcium, thin filaments, and the integrative biology of cardiac contractility. *Annu Rev Physiol* 67: 39–67, 2005.
21. **Kuwahara F, Kai H, Tokuda K, Takeya M, Takeshita A, Egashira K, Imaizumi T.** Hypertensive myocardial fibrosis and diastolic dysfunction: another model of inflammation? *Hypertension* 43: 739–745, 2004.
22. **Landmesser U, Drexler H.** Chronic heart failure: an overview of conventional treatment versus novel approaches. *Nat Clin Pract Cardiovasc Med* 2: 628–638, 2005.
23. **Lee SD, Kuo WW, Lin JA, Chu YF, Wang CK, Yeh YL, Wang SG, Liu JY, Chang MH, Huang CY.** Effects of long-term intermittent hypoxia on mitochondrial and Fas death receptor dependent apoptotic pathways in rat hearts. *Int J Cardiol* 116: 348–356, 2007.
24. **Levy D, Garrison RJ, Savage DD, Kannel WB, Castelli WP.** Prognostic implications of echocardiographically determined left ventricular mass in the Framingham Heart Study. *N Engl J Med* 322: 1561–1566, 1990.
25. **Manso AM, Elsherif L, Kang SM, Ross RS.** Integrins, membrane-type matrix metalloproteinases and ADAMs: Potential implications for cardiac remodeling. *Cardiovasc Res* 69: 574–584, 2006.
26. **McGuire M, Bradford A.** Chronic intermittent hypoxia increases haematocrit and causes right ventricular hypertrophy in the rat. *Respir Physiol* 117: 53–58, 1999.
27. **McGuire M, Bradford A.** Chronic intermittent hypercapnic hypoxia increases pulmonary arterial pressure and haematocrit in rats. *Eur Respir J* 18: 279–285, 2001.
28. **Nicoletti A, Michel JB.** Cardiac fibrosis and inflammation: interaction with hemodynamic and hormonal factors. *Cardiovasc Res* 41: 532–543, 1999.
29. **Park AM, Suzuki YJ.** Effects of intermittent hypoxia on oxidative stress-induced myocardial damage in mice. *J Appl Physiol* 102: 1806–1814, 2007.
30. **Parish JM, Somers VK.** Obstructive sleep apnea and cardiovascular disease. *Mayo Clin Proc* 79: 1036–1046, 2004.
31. **Roos KP.** Mechanics and force production. In: *The Myocardium* (2nd ed.), edited by Langer GA. San Diego, CA: Academic, 1997, p. 235–323.
32. **Sabri A, Hughie HH, Lucchesi PA.** Regulation of hypertrophic and apoptotic signaling pathways by reactive oxygen species in cardiac myocytes. *Antioxid Redox Signal* 5: 731–740, 2003.
33. **Scharf SM, Chen L, Greenburg H, O'Donnel CP.** Cardiovascular response to obstructive apneas: lessons from animal models. In: *Respiratory-Circulatory Interactions in Health and Disease,* edited by Scharf SM, Pinsky M, Magdar S. New York: Dekker, 2001, p. 613–740. (Lung Biol Health Dis Ser).
34. **Shorofsky SR, Aggarwal R, Corretti M, Baffa JM, Strum JM, Al-Seikhan BA, Kobayashi YM, Jones LR, Wier WG, Balke CW.** Cellular mechanisms of altered contractility in the hypertrophied heart: big hearts, big sparks. *Circ Res* 84: 424–434, 1999.
35. **Sica AL, Greenberg HE, Scharf SM, Ruggiero DA.** Chronic-intermittent hypoxia induces immediate early gene expression in the midline thalamus and epithalamus. *Brain Res* 883: 224–228, 2000.
36. **Takemura G, Fujiwara H.** Role of apoptosis in remodeling after myocardial infarction. *Pharmacol Ther* 104: 1–16, 2004.
37. **Xia Y, Javadov S, Gan TX, Pang T, Cook MA, Karmazyn M.** Distinct K_{ATP} channels mediate the antihypertrophic effects of adenosine receptor activation in neonatal rat ventricular myocytes. *J Pharmacol Exp Ther* 320: 14–21, 2007.
38. **Xu W, Chi L, Row BW, Xu R, Ke Y, Xu B, Luo C, Kheirandish L, Gozal D, Liu R.** Increased oxidative stress is associated with chronic intermittent hypoxia-mediated brain cortical neuronal cell apoptosis in a mouse model of sleep apnea. *Neuroscience* 126: 313–323, 2004.